Nanotechnol. Environ. Eng. (2017) 2:8
https://doi.org/10.1007/s41204-017-0018-7

ORIGINAL PAPER

Phytoextract-mediated synthesis of zinc oxide nanoparticles using aqueous leaves extract of *Ipomoea pes-caprae* (*L*).*R.br* revealing its biological properties and photocatalytic activity

Alagesan Venkateasan[1] · Rangasamy Prabakaran[1] · Venugopal Sujatha[1]

Received: 13 December 2016 / Accepted: 29 May 2017 / Published online: 7 June 2017

Abstract ZnO NPs were efficiently synthesized from the leaves extract of *Ipomoea pes-caprae*. The work focuses on phytochemical studies, phytomediated synthesis and characterization of ZnO NPs and its biological applications. Phytochemicals present in the extract may be responsible for reducing the metal salts into their respective nanosize particles. The UV–Vis spectrum infers the formation of NPs, with absorbed peak at 322 nm. The XRD pattern depicted significant peaks at 2θ positions which confirmed the hexagonal wurtzite structure. FTIR spectrum (ZnO NPs) was recorded to identify the functional group of biomolecules involved in synthesis. ZnO NPs was measured in the range of 2–20 nm by FE-SEM and particle analyses. ZnO NPs in various concentrations revealed potential antioxidant (IC_{50}-21.09) and antibacterial activities. Cytotoxicity activity by Vero cell line (MTT assay) was found to be significant. ZnO NPs exhibited concentration-dependent cytotoxic reactivity to Vero cells after 24-h contact. ZnO NPs exhibited efficient dye degradation of methylene blue in the presence of sunlight. Due to the versatile properties and applications of ZnO NPs, these were widely studied by user-friendly approaches being green, simple and economy.

✉ Venugopal Sujatha
chemsujatha888@gmail.com

[1] Phytochemistry Lab, Department of Chemistry, Periyar University, Periyar Palkalai Nagar, Salem, Tamil Nadu 636 011, India

Graphical Abstract

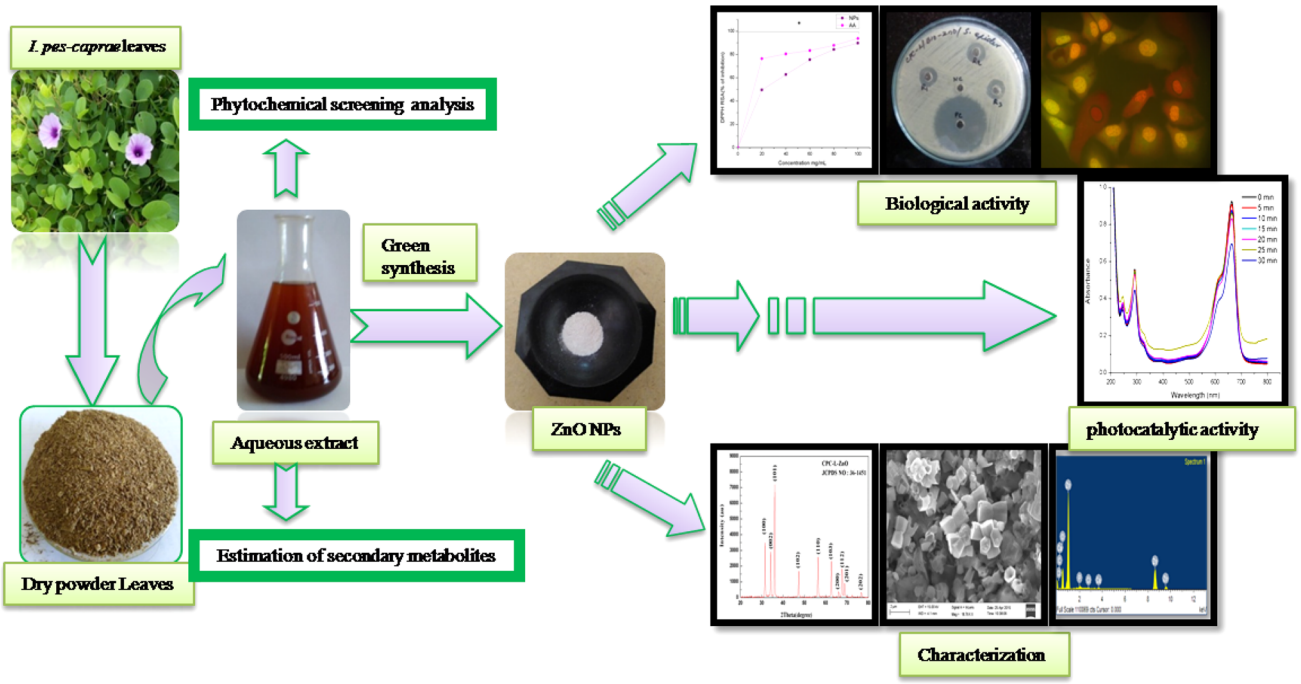

Keywords *I. pes-caprae* · ZnO NPs · Antibacterial · MTT assay · Photocatalytic activity

Introduction

The nature has provided the warehouse of medicine to cure numerous ailments of human beings. Medicinal plants contain active constituents that are used in the treatment of multiple human diseases [1, 2]. Nowadays, the growth of nanotechnology has opened up a world of new possibilities for fabricating nanomaterials with wide range of applications [3]. Nanomaterials are used in intracellular delivery of RNA, DNA, proteins, peptides and drugs for inducing cancer cell death and as contrast agents for cancer imaging [4]. Cancer is one of the leading causes of death worldwide and characterized by proliferation of abnormal cells. Nanoparticles (NPs) can offer unique interactions with biomolecules and may be useful in cancer diagnosis and treatment [5]. The fight against cancer is difficult particularly in the development of therapies for severely multiplying tumors. So, conventional methods require the combination of controlled released technology and targeted drug delivery which is more effective and less harmful. Nanomaterials are expected hopefully to revolutionize cancer diagnosis and therapy [6]. The zinc ions might explain ZnO-induced cytotoxic and apoptotic activity. Zinc ions released from ZnO materials induce oxidative stress-mediated cell death [7–9], and the strong correlation between ZnO NPs-induced cytotoxicity and free zinc ion concentration also suggests a requirement for ZnO dissolution for effective cytotoxicity [10]. A number of studies have reported the toxicity of ZnO materials, and their potential to induce cell death has been explored in cancer biology [7, 11].

Syntheses of nanoparticles were one of current biomedicine production process from the medicinal plants [12]. The plant extracts act as a capping agent for nanoparticles synthesis and are now valuable over other biological processes [13]. Biological process for nanoparticle synthesis using bacteria, fungi, enzymes, plants, algae, collagen, macromolecules and amino acid sequences has been proposed as eco-friendly alternatives to chemical and physical methods [14–16]. Green synthesis was acquiring high interest based on the rich content of active metabolites in plant [17]. The metal oxides have a higher portion of atoms and liable for their potential properties such as magnetic, electronic and antimicrobial activity [18]. Many environmental pollutants are organic in nature, and many proposed methods of environmental decontamination involve oxidation of the organic pollutants [19]. However, using semiconductor photocatalysts to oxidize and remove such pollutants from the local environment has many advantages over alternative methods [20]. Nanoparticles have a high surface area per volume, which increases the number of available surface states to serve as reaction sites. However, increased crystallinity associated with larger particle sizes typically results in greater optical efficiency and therefore

higher electron–hole pair production efficiency [21, 22]. ZnO was an important photocatalyst due to its unique advantages and using semiconductors photocatalysts for the removal of organic pollutants in wastewater [23]. The photocatalytic effects of ZnO are being exploited for use within self-cleaning paints, in environmental remediation applications and prophylactics with nanoparticle and colloidal suspensions demonstrating high photodegradation efficiency for organic compounds [24]. In photocatalytic reactions, the semiconducting materials can use sunlight energy to degrade organic pollutants into nontoxic compounds in aqueous solution, viewing considerable potentials for purifying dye-contaminated water as a green system [25]. Besides, the recent findings showed that metal nanoparticles were successfully used in the degradation of color dyes. Thus, plant extract-mediated synthesis of metal nanoparticles can be economy and simple when compared with chemical and physical method [26, 27]. ZnO NPs are widely used due to their unique antibacterial, antifungal, high catalytic and photochemical activities [28, 29].

Ipomoea pes-caprae Linn. (F: Convolvulaceae) is commonly called as "Beach Morning Glory or Goat's Foot." It occurs along with the beaches, strands and tropical islands of tropical North and South America, India, Asia and Australia [30]. *Ipomoea pes-caprae* (*I. pes-caprae*) has been reported to scavenge free radicals and can be an essential source of antioxidants [31]. The leaves extract has astringent, diuretic and laxative properties, and it possesses biological activity like anticancer, antioxidant, anti-inflammatory, antispasmodic, antinociceptive and hypoglycemic properties [32]. *I. pes-caprae* is highly reputed in folk and tribal medicines. Hence, the current study was intended to use *I. pes-caprae* as a bioreductant and capping agent for the synthesis of ZnO nanoparticles as a hopeful carrier and to evaluate its biological applications and photocatalytic activity.

Materials and methods

Plant collection and materials

Healthy *I. pes-caprae* leaves were collected from Sarabanga River, Omalur, Salem district, Tamil Nadu, India. The plant materials were identified and confirmed by Botanical Survey of India (BSI), Coimbatore, Tamil Nadu, India. The voucher specimen number is BSI/SRC/5/23/2014-15/Tech.1458.

Zinc acetate dihydrate [Zn $(CH_3COO)_2{\cdot}2H_2O$], sodium hydroxide and all chemicals used were analytical grade, purchased from Merck and used without further purification. Distilled and sterile deionized water was used in all experimental work.

Preparation of plant leaves extract

I. pes-caprae leaves were washed several times with sterile distilled water to remove dust particles and then shade dried. *I. pes-caprae* leaves extract was prepared by placing 10 g of dried fine cut in 500-mL glass beaker along with 500 mL of sterile distilled water. The mixture was then boiled for 15 min until the color of aqueous solution changed from aqueous to yellow. Then, the mixture was cooled to room temperature and filtered with Whatman No.1 filter paper before centrifuging at 1200 rpm for 2 min to remove biomaterials. The extract was stored at room temperature in order to be used for further experiments.

Phytochemical analysis

Qualitative phytochemical analysis

Phytochemical screening The preliminary phytochemical screening analysis was carried out according to method of Onwukeame et al. [33].

Quantitative phytochemical analysis

Determination of total phenol content The total phenol content in the aqueous extract of *I. pes-caprae* was estimated by spectrophotometric assay [34]. The results were expressed as μg of gallic acid equivalents/mg of extract (GAEs).

Determination of total flavonoid content Flavonoid content in the aqueous extract *I. pes-caprae* was determined by spectrophotometric method [34]. The results were expressed as μg of (±)-catechin equivalents (CEs) per mg of extract.

Estimation of total flavonol content Total flavonols were determined by using rutin as a reference compound. This method is based on the formation of complex with maximum absorption at 440 nm [35]. The results were expressed as μg of rutin equivalents per mg of extract.

Estimation of tannin content Tannin content of the aqueous extract *I. pes-caprae* was measured by Folin–Denis method [36]. The results were expressed as μg of tannic acid equivalents per mg of extract.

Synthesis of zinc oxide nanoparticles

Ten mL of the aqueous yellow leaf extract of *I. pes-caprae* was added to 500 mL of 50 mM of aqueous zinc acetate dihydrate solution and stirred at room temperature for 20 min to achieve a pale yellow solution. The suspended particles were purified by dispersing in sterile distilled

water and centrifuged thrice. The pale white particles obtained were washed with ethanol to remove the impurities from the final product. Then, a white powder was obtained after drying at 60 °C in vacuum oven for 6 h [37].

Characterization techniques

UV–visible spectroscopy

ZnO was characterized in a Perkin-Elmer UV–Vis spectrophotometer Lambda-19 to know the kinetic behavior of ZnO NPs. The scanning range of the samples was 200–800 nm at a scan speed of 480 nm/min. The spectrophotometer was equipped with "UV Winlab" software to record and analyze data. The UV–Vis absorption spectrum of the samples was recorded, and numerical data were plotted in the "Origin 8."

Fourier transforms infrared spectroscopy (FTIR)

Two mg of the extract or NPs was encapsulated in 100 mg of KBr pellet, in order to prepare translucent sample disks. The pelleted sample specimens were treated for FTIR spectroscopy (Brucker IR Affinity, Japan) in the range of wavelength 400–4000 cm^{-1} with a resolution of 1 cm^{-1}. The FTIR spectrum was recorded in Perkin-Elmer spectrophotometer.

X-ray diffraction (XRD)

The crystalline size and purity were characterized by X-ray diffractometer (Philips PAN analytical) using Cu-Kα radiation of wavelength $\lambda = 1.541$ Å of synthesized ZnO NPs. The particle size of the prepared samples was determined by using the Scherrer's equation as follows: $D \approx 0.9/\cos\theta$, where D is the crystal size, λ is the wavelength of X-ray, θ is the Braggs angle in radians and B is the full width at half maximum of the peak in radians.

Particle size analysis

The particle size of the ZnO NPs was determined by a laser diffraction apparatus (NANOPHOX). NANOPHOX is an innovative photon cross-correlation sensor allowing for simultaneous measurement of particle size and stability of opaque emulsions and suspensions in the nanometer regime. The sizes of the ZnO NPs were analyzed using light scattering at room temperature (25 ± 2 °C).

Field emission scanning electron microscope (FE-SEM) and EDX

The morphology of the synthesized ZnO NPs was observed by field emission scanning electron microscopy (FE-SEM), and the elemental analysis of composition was recorded by the instrument of ZEISS EVO-MA 10, Oberkochen, Germany.

Biological applications

Antioxidant activity

DPPH radical scavenging activity The DPPH radical scavenging activity was carried out according to the method of Patra et al. [17]. The IC_{50} values of the ZnO NPs, i.e., concentration of ZnO NPs necessary to decrease the initial concentration of DPPH by 50%, were calculated.

Antibacterial activity The antibacterial ability of synthesized ZnO NPs was evaluated using agar well diffusion method, as per the modified protocol of Srinivasan et al. [38].

Cytotoxicity studies

The Vero cell line was obtained from National Centre for Cell Sciences Repository, University of Pune, India. Vero cells were maintained in a humidified atmosphere containing 5% CO_2 at 37 °C in *Dulbecco's modified Eagle's* medium (DMEM) supplemented with 100 units of penicillin, 100 µgm/L of streptomycin and 10% fetal bovine serum (FBS). Briefly, Vero cell was precultured in 96-well microtiter plates for 48 h under 5% CO_2.

The cytotoxicity activity of synthesized ZnO NPs was determined by the MTT (3-[4,5-methylthiazol-2-yl]-2,5-diphenyl-tetrazolium bromide) assay using Vero cells [39].

Apoptotic assay by acridine orange/ethidium bromide (AO/EB) staining method

Apoptotic studies were performed with a staining method utilizing AO and EB. The cells were seeded at a density of 1 × 106 cells/well. After attachment, the Vero cells were treated with ZnO NPs (50 µM) and incubated for 24 h at 37 °C in CO_2 incubator. After the treatment period, the cells were washed with ice-cold phosphate-buffered saline (PBS). Both AO/EB was added at a concentration of 1 mg/mL. The Vero cells were mounted on a slide, and the images were observed under a fluorescent microscope [40–42].

Sunlight-induced photocatalytic activity

The photocatalytic activity of plant-mediated synthesized ZnO NPs was determined by degradation of methylene blue (MB) under sunlight irradiation [43].

Statistical analysis

Statistical analyses were done using the SPPS software (16.0 version). Analysis of variance (ANOVA) in a completely randomized design and Tukey's multiple range tests was used to compare the significant differences between samples. Values were expressed as mean ± standard deviation. All determinations were done at least in triplicate, and all were averaged. The confident limits used in this study were based on 95% ($p < 0.05$).

Results and discussion

Qualitative phytochemical analysis

Phytochemical screening

The aqueous leaves extract of *I. pes-caprae* possess a variety of bioactive constituents such as alkaloids, flavonoids, flavonols, glycosides and tannins (Table 1). They were screened by qualitative phytochemical screening, and the bioactive constituents present may be responsible for reducing the metal salts into their respective nanosize particles [44].

Table 1 Phytochemical screening of *I. pes-caprae* aqueous leaves extract

S. no	Phytochemical constituents	Aqueous extract
1.	Flavonoids	++
2.	Flavonal	+++
3.	Phenolics	+++
4.	Tannin	+++
5.	Amino acids	++
6.	Steroids	+
7.	Proteins	+++
8.	Carbohydrates	++
9.	Saponins	−
10.	Terpenoids	+

+++, copiously present; ++, moderately present; +, slightly present; −, absent

Quantitative phytochemical analysis

The plant secondary metabolites like total phenolic, flavonoids, flavonol, tannins, content of *I. pes-caprae* aqueous leaves extract are depicted in Table 2. The phenolic compounds present in the *I. pes-caprae* leaves aqueous extract are estimated by using gallic acid as standard. The total phenolic content of aqueous leaves extract is in the range of 13.59 ± 0.78 µg/mL. The flavonoid content of *I. pes-caprae* aqueous leaves extract was observed by using catechin equivalent. The aqueous leaves extract recorded the amount of flavonoid content to be 117.00 ± 2.81 µg/mL. The flavonoid content rich in the extract is encouraging stabilization of the metal nanoparticles due to their electron-donating capability and capping property of the flavonoid compound. The total flavonol content in *I. pes-caprae* aqueous leaves extract was found to be 8.44 ± 0.32 µg/mL. The phytoextract-mediated synthesis of metal nanoparticle may infer its antioxidant potential due to deposition of bioactive compounds on their surface. Leaves extract has measurable quantities of tannin content in the range of 13.00 ± 3.33 µg/mL. The tannin content may be supportive to enhance the stabilization of the metal nanoparticles. Secondary metabolites in plant source of therapeutic importance compared to bacteria and fungi thereby provide greater scope for the fabrication of biocompatible nanoparticles [45]. From the above results, the leaves aqueous extract of *I. pes-caprae* possesses enormous phytoconstituents to synthesize the ZnO NPs from the reduction in zinc acetate salt by green route.

Synthesis of zinc oxide nanoparticles

I. pes-caprae aqueous leaves extract was added to aqueous zinc acetate dihydrate solution and stirred for 1 h and dried. The pale white color of the ZnO NPs arises due to capping action of biomolecules of *I. pes-caprae* leaves extract on the surface of the nanoparticles. The suspended particles were purified by dispersing in sterile distilled

Table 2 Total phenolic, flavonoids, flavonol, tannins, content of *I. pes-caprae* aqueous leaves extract

S. no	Phytochemical constituents	*I. pes-caprae* leaves aqueous extract	
		Absorbance (nm)	Content (µg/mg)
1.	Total phenolic	0.245 ± 0.010	13.59 ± 0.78^{b}
2.	Total flavonoid	0.475 ± 0.012	117.00 ± 2.81^{a}
3.	Total flavonol	0.122 ± 0.003	08.44 ± 0.32^{d}
4.	Total tannins	0.013 ± 0.001	$13.00 \pm 3.33^{b,c}$

Data represent the mean ± SD (n = 3). Mean values of each row followed by different superscript letters (a–c) significantly differ when subject to Tukey's multiple comparison test ($p < 0.05$)

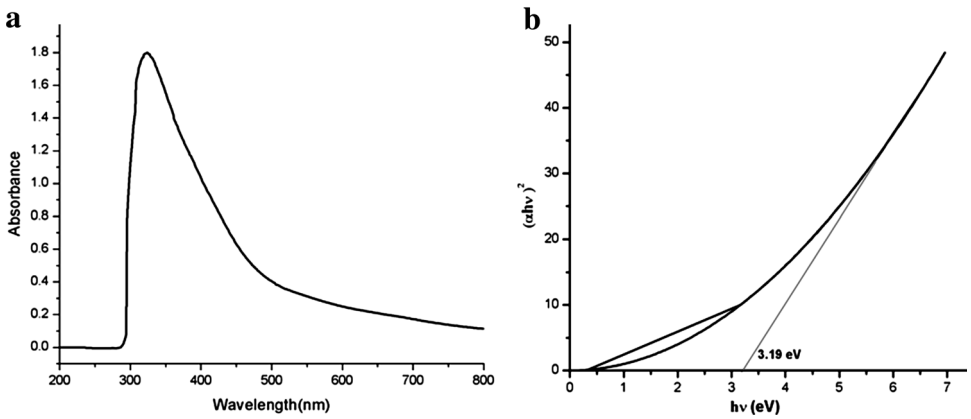

Fig. 1 **a** The UV–Vis absorption spectra and **b** band gap energy of ZnO nanoparticles

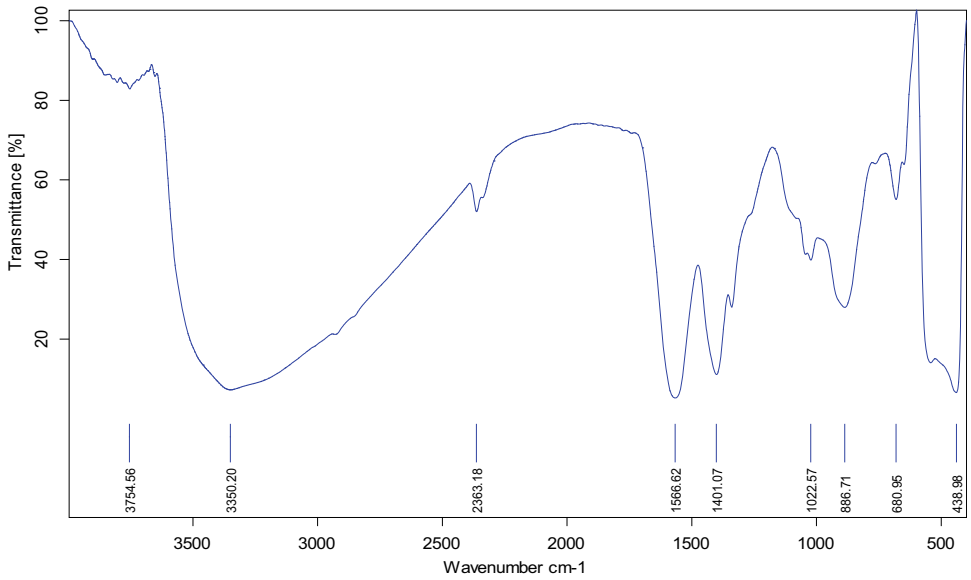

Fig. 2 FTIR spectra of ZnO NPs using *I. pes-caprae* leaf aqueous extract

water and centrifuged thrice. The pale white particles obtained were washed with ethanol to remove the impurities from the final product. Then, a white powder was obtained after drying at 60 °C in vacuum oven for 6 h.

Characterization techniques

UV–Vis spectral analysis

UV–visible spectroscopy used to identify the synthesis of ZnO NPs Fig. 1a represents the formation of ZnO NPs. Freshly prepared ZnO suspensions in plant extract exhibit a strong absorption at 322 nm in the UV region. This surface plasmon resonance band undergoes a red- or blueshift, depending on the quantum size effects. The absorbance of ZnO NPs depends on their shape and size [27]. The plant extract react with Zn^{2+} ions reduces the precursor solution and formation of nanoparticles monitored by UV–visible spectroscopy. This absorption value that corresponds to the near 3.76 eV band gap is greater than the bulk band gap of 3.2 eV. The bulk ZnO NPs maximum absorption usually occurs around 385 nm. ZnO NPs have given the band gap of 3.1 eV in Fig. 1b, and this band gap energy is near to the bulk band gap energy. This proves that the zinc ion is efficiently reduced by the *I. pes-caprae* aqueous extract.

FTIR analysis

In this way, the presence of biomolecules in the aqueous extract which was responsible for the reduction and stabilization of the synthesized nanoparticles can be identified. The FTIR spectrum of the *I. pes-caprae* aqueous leaf extract-mediated synthesized ZnO NPs is shown in Fig. 2.

In the FTIR spectrum of *I. pes-caprae*, aqueous leaf extract synthesized ZnO NPs which showed a broad peak at 3350 cm^{-1} is due to stretching vibrations of N–H groups of hydrogen bond and a sharp peak at 3400–3250 cm^{-1} leads to N–H stretching for primary and secondary amines. A small peak appeared at 3754 cm^{-1} which is closer to 3700 cm^{-1} wavenumber indicates free O–H group. The

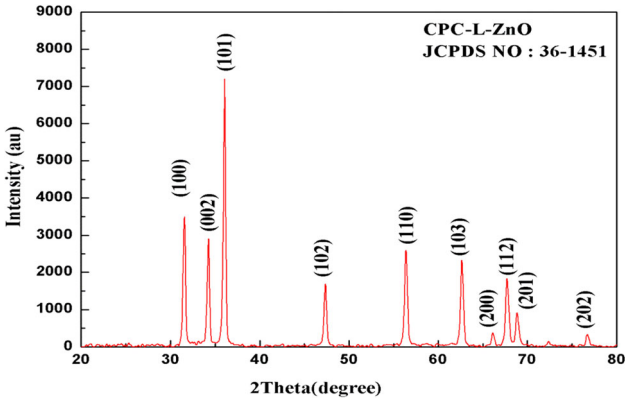

Fig. 3 XRD spectra of ZnO NPs using *I. pes-caprae* leaf aqueous extract

sharp peak at 1500–1411 cm^{-1} implies an aromatic ring shows the C–C stretching in aromatic ring. Little sharp peak at 2363 cm^{-1} arises among the wavenumber of 2700–2250 cm^{-1} indicating the presence of amino acid N–H stretching. 1022 cm^{-1} peak by C–O stretching reveals alcohols, carboxylic acids, esters, ethers. Finally the weak band at 886 cm^{-1} is the result of C–H out of plane bending. The peak 895–875 cm^{-1} represented the compounds such as polyphenols, carboxylic acid, polysaccharide, amino acid and proteins. The IR spectrum revealed the presence of active compounds in leaf aqueous extract of *I. pes-caprae* which may be significant for ZnO NPs stabilization. Earlier report showed that the phenolic groups of molecules are responsible for the reduction process and the stability of ZnO NPs is due to the free amino and carboxylic groups [46].

XRD analysis

The XRD spectra of *I. pes-caprae* leaf aqueous extract-mediated ZnO NPs are shown in Fig. 3. The prominent peaks corresponding to the diffraction planes (100), (002), (101), (102), (110), (103), (200), (112), (201) and (202) agreed well with the JCPDS Card No. 36-1451, confirming the hexagonal wurtzite structure of the ZnO NPs. The strong intensity and broadened diffraction peaks clearly indicate that the ZnO NPs is highly crystalline in nature. Similar results are obtained by Yu et al. [47]. The average particle size (D) of synthesized nanoparticles was calculated using the well-known Scherrer formula $D = 0.9\ \lambda/\beta \cos\theta$, where λ is the wavelength of X-ray source (Cu-Kα line—0.1541 nm), β is the full width at half maximum (FWHM) in radians and θ is Bragg's diffraction angle. The calculated value of D was 25 nm.

Particle size analysis

The size of the particles was determined by particle size analyzer (Fig. 4). Sizes of phytoextract-mediated synthesis of ZnO NPs were ranging from 10 to 100 nm. Size distribution histogram (Fig. 6) of ZnO NPs confirmed that particles were well distributed in the solution.

FE-SEM analysis

FE-SEM image (Fig. 5) reveals the particle size and external morphology of the ZnO NPs. It can be seen from the image that the ZnO NPs ranges from 2 to 20 nm. Nanoparticles in profile have been agglomerated into bigger ones. Profile confirms the structure of nanodumbbell of which is in close agreement with green method.

The EDX reveals that the required phase is present. Both zinc (Zn) and oxygen (O) are present in the sample (Fig. 7), and peaks of zinc and oxygen elements 65.85% and 28.33%, respectively, prove ZnO NPs synthesized low of impurity. The graph also shows that the presence of carbon (C), chlorine (Cl), phosphorus (P) and calcium (Ca)

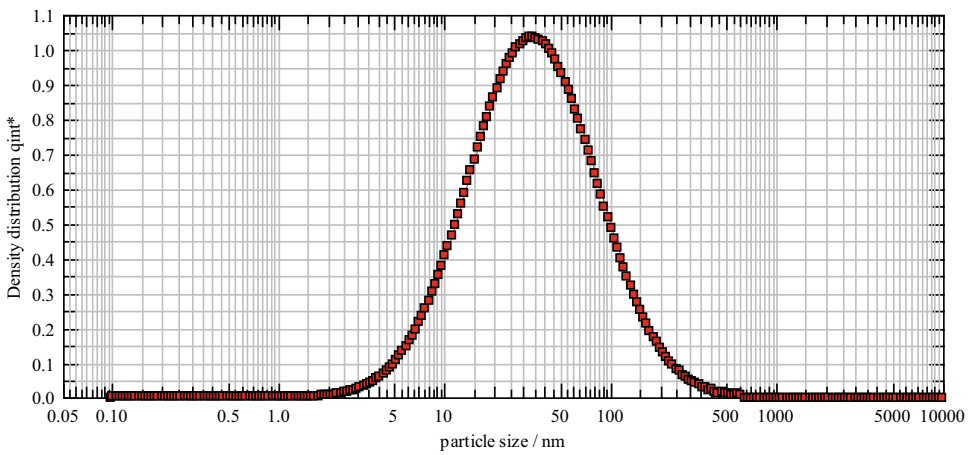

Fig. 4 Particle size of ZnO nanoparticles

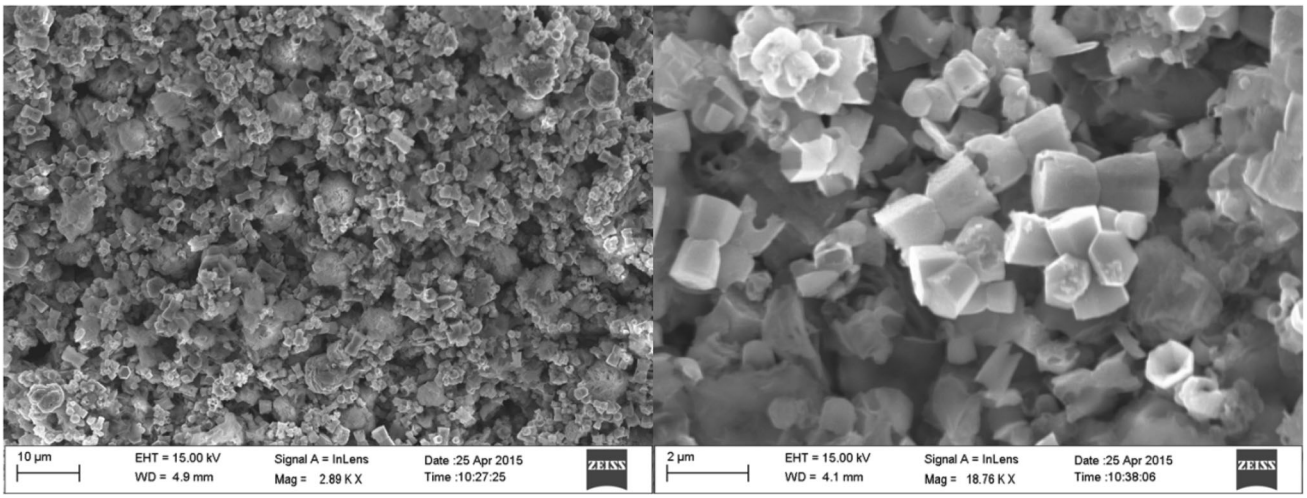

Fig. 5 FE-SEM images of ZnO nanoparticles

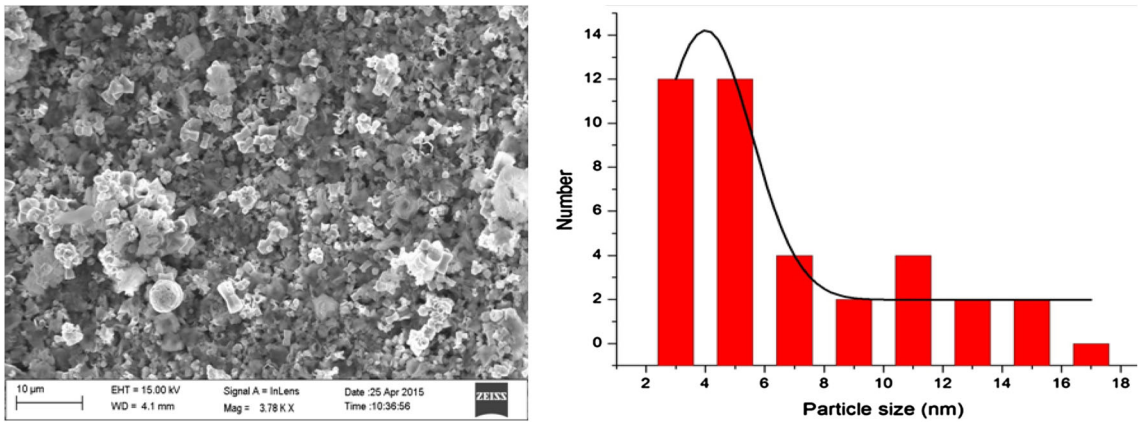

Fig. 6 Size distribution curve

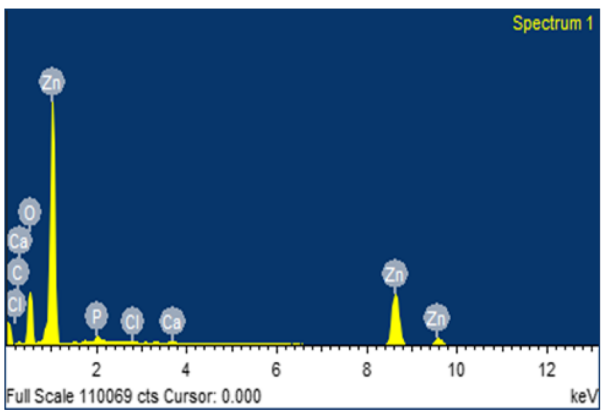

S. No	Element	Weight %	Atomic %
1	C	3.88	10.23
2	P	1.31	1.34
3	Cl	0.18	1.16
4	Ca	0.46	0.36
5	Zn	65.85	31.88
6	O	28.33	56.04

Fig. 7 EDX spectra of ZnO nanoparticles

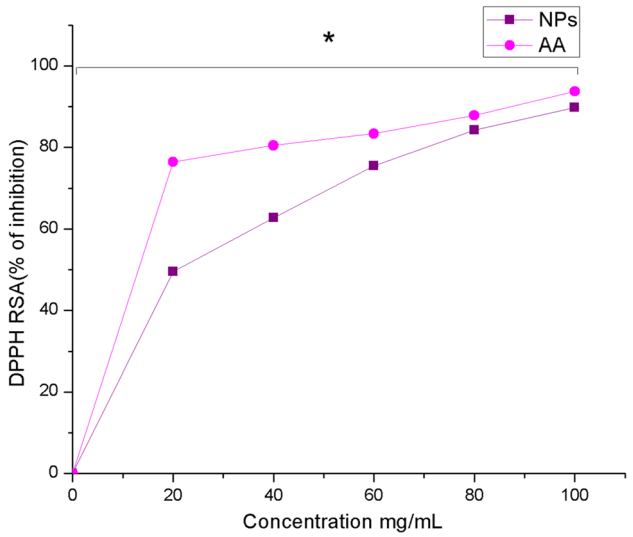

Fig. 8 DPPH radical scavenging activity

is present in the EDX picture in less amounts. This is probably due to the presence of substrate over which the nanoparticle sample was held during SEM microscopy.

Biological applications

Antioxidant activity of ZnO nanoparticles

The antioxidant activities of ZnO NPs are portrayed in Fig. 8. The DPPH free radical scavenging activity of ZnO NPs at 20–100 µg/mL ranged from 49.56 to 89.73%, whereas the scavenging activity of the standard ascorbic acid ranged from 76.45 to 93.75%. The DPPH assay demonstrated significant radical scavenging activity of ZnO NPs having an IC_{50} value of 21.09 µg/mL, when compared with the IC_{50} value of ascorbic acid 13.14 µg/mL. Phytochemical analysis signifies that *I. pes-caprae* leaves possess enormous bioactive constituents and higher amount of metabolites present. It is well known and also reported in the previous literature that plant-mediated NPs synthesis involves sequential reduction followed by capping with these plant constituents [48]. Previous studies on ZnO nanopellets exhibited significant activity (IC_{50} value 11.40 µg/mL) at higher concentration. ZnO NPs synthesized by *O. tenuiflorum* act as potential antioxidants [49]. Nanoparticles of gold [50], silver [51], selenium [52] and copper oxide [53] are known to exhibit free radical scavenging activity. Thus, the antioxidant activity of ZnO NPs may be attributed to the functional group adhered.

Antibacterial activity of ZnO NPs

Synthesized ZnO NPs were analyzed by disk diffusion method using selected organisms such as *S. epidremidies,* E. *coli, S. typhi* and *S. aureus.* As the concentration of ZnO NPs increases, the zone of inhibition also increased against the bacteria strain is shown in (Table 3). The antibacterial effect of ZnO NPs has been reported against Gram-positive and Gram-negative bacteria due to the larger surface area and electrostatic interaction of nanoparticles.

In our present investigation, the antibacterial activities of ZnO NPs were determinate against Gram-positive bacteria's like *S. epidremidies* and *S. aureus* and Gram-negative bacteria's like *E. coil* and *S. typhi*. The bacteria were maintained on a nutrient broth (NB) at 37 °C. ZnO NPs exhibited potent antibacterial activity against listed organisms as shown in Table 3. When tested by the disk diffusion method, ZnO NPs exhibited significant activity against *S. epidremidies* and *S. aureus* with zone of inhibition 13 and 11 mm. The higher zone of inhibition observed in *E. coli* and *S. typhi* 14 mm by ZnO NPs may (efficiency of *E. coil* and *S. typhi* pathogens) serve as an antibacterial agent. This proves that the ZnO NPs synthesized by the simple solution method may be used for microbial activity study.

Determination of cytotoxic effect of ZnO NPs

MTT assay [3-(4,5-dimethyl-2-thiazolyl)-2,5-diphenyl-2H-tetrazolium bromide] was carried out to determine the in vitro cytotoxic effect of synthesized ZnO NPs. One plate of Vero cells was treated with concentrations of 10–1000 µg/mL of synthesized ZnO NPs, and other plate was untreated. Both were subjected to 48 h of incubation to the study the inhibitory percentage. The cell viability was decreased by increasing the concentrations of the ZnO NPs.

Table 3 Antibacterial activity of ZnO NPs

S. no	Bacteria	Organisms	Diameter of zone of inhibition (in mm)[c]		
			Zinc oxide NPs	Positive control[a]	Negative control[b]
1	Gram-positive bacteria	*S. epidremidies*	13.00 ± 1.00	35.00 ± 2.16	00.00 ± 0.00
2		*S. aureus*	11.33 ± 0.57	22.50 ± 1.00	00.00 ± 0.00
3	Gram-negative bacteria	*E. coil*	14.00 ± 0.00	22.00 ± 0.81	00.00 ± 0.00
4		*S. typhi*	14.00 ± 0.00	31.50 ± 1.00	00.00 ± 0.00

[a] Ciprofloxacin (1 mg/mL); [b] DMSO (50 µl/well); [c] the values are mean of triplicates with (±) standard deviation (mean ± SD; $n = 3$)

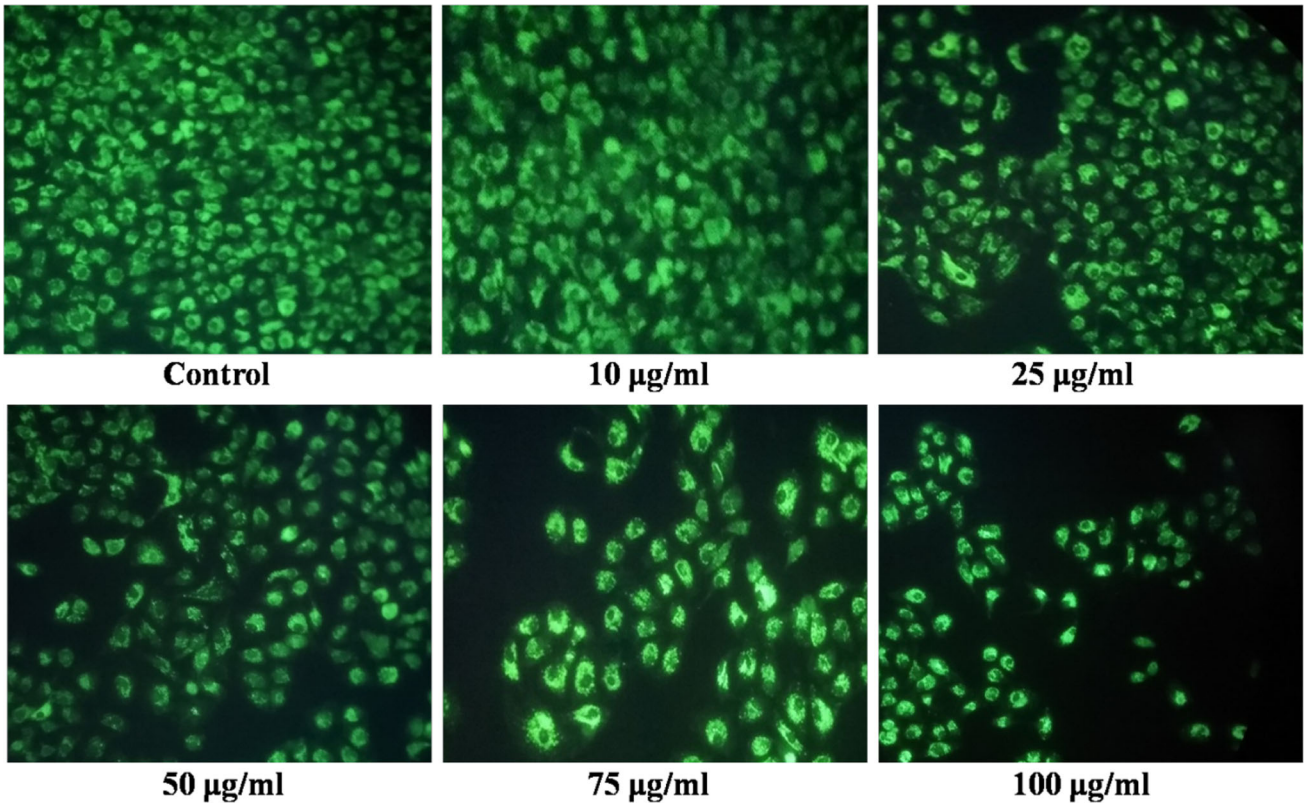

Fig. 9 Cytotoxicity activity of ZnO nanoparticle by MTT assay

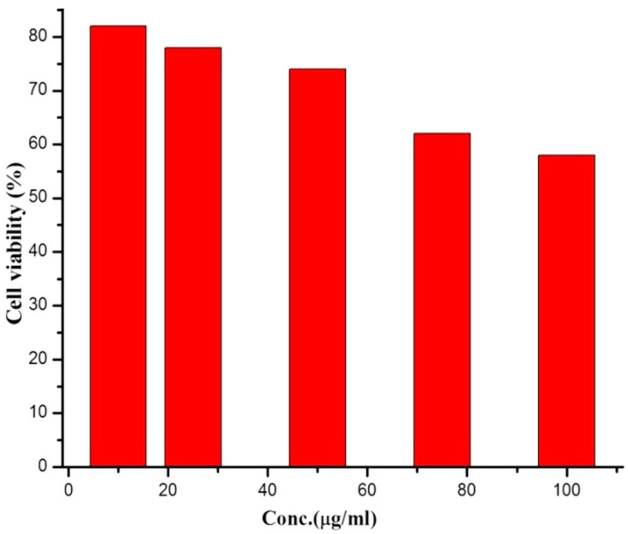

Fig. 10 Cell viability of ZnO nanoparticles

The IC_{50} values of the Vero cells are shown in Fig. 10. Nanoparticles exhibit significant cytotoxicity at their lower concentrations, and cytotoxicity increases with increased concentrations at 10–1000 µg/mL. The change in morphology is depicted in Fig. 9.

The most identifiable morphological changes of ZnO NPs-treated cells observed in this study were cytoplasmic condensation, cell shrinkage and production of numerous cell surface swelling in the plasma membrane. The mortality data obtained in this study allowed us to estimate nanoparticle ability not only the reason as that of cytotoxic agent, but also in terms of the potential reduction in tumor growth. The cytotoxic effects of silver and ZnO NPs resulted due to the active phytochemicals (functional groups) interaction of metal atoms with intracellular proteins, as well as the nitrogen bases in DNA [54]. Recently, reports show that the IC_{50} value of ZnO NPs was 62.5 µg/mL against Vero cell lines [55, 56]. In contrast, the synthesized ZnO NPs showed higher rates of cytotoxicity against Vero cells at 50.04 (µg/mL).

Vero cells treated at an increasing concentration of ZnO NPs for 24 h to check for Fig. 9 clearly illustrate that ZnO NPs at concentrations of 10, 25, 50, 75, 100 µg/mL did not show any cytotoxicity to the normal cell line (Vero). MTT results showed that ZnO NPs significantly decreased the viability of Vero in a dose-dependent manner. At 75 µg/mL, cell viability was significantly decreased to 62% for the Vero cells as shown in Fig. 10.

Generally, two types of cell death are: necrosis (accidental cell death) and apoptosis (programmed cell death) [57]. Apoptotic cells are transformed into small membrane-bound vesicles, and no inflammatory response is found [58]. The AO/EB staining assay can detect the difference in

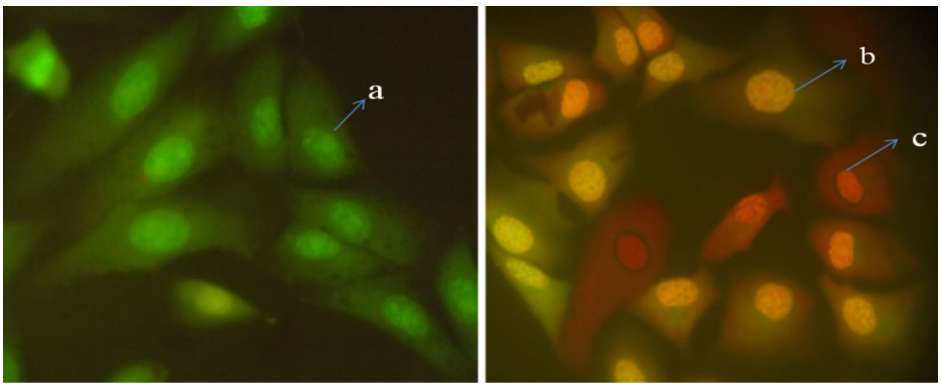

Fig. 11 Analysis of cell death induced by ZnO NPs identified by AO/EB staining. Vero cells without treatment (**A**) and in the presence of ZnO NPs (**B**). Vero cells were treated with ZnO NPs (50 μM) and incubated for 24 h at 37 °C. Cells in *a*, *b* and *c* are living, apoptotic and necrotic cells, respectively

membrane integrity between necrotic and apoptotic cells. AO is a vital dye and can stain both live and dead cells. EB stains only cells that have lost their membrane integrity. Figure 11 clearly shows that control cells are viable and uptake the dye acridine orange (cells appear bright green with normal cell morphology), whereas the cells treated with ZnO NPs uptake the dye ethidium bromide and appear red orange with cell shrinkage indication of cell death. So the ZnO NPs were found to induce the cell death by necrosis. Hence, the result reveals that the ZnO NPs have significant anticancer properties against Vero cell lines.

It is interesting to note that the ZnO NPs showed high level of cytotoxic activity against the tested cancer cell lines. It may be suggested that the synthesized ZnO NPs would play a major role in target-based bioactive molecules into specific cancer cells.

Sunlight-induced Photocatalytic activity of synthesized ZnO NPs

The synthesized ZnO NPs degradation activity against MB is shown in Fig. 12. The optimum absorbance peak of MB is 667 nm. The photocatalytic degradation of MB in the incidence of ZnO NPs was envisaged by a decrease in peak intensity within 30 min of incubation under sunlight. The color dye degradation is mainly accredited to the size, morphology and surface charge property of the synthesized ZnO NPs. Photon-induced molecular reactions occur at the surface of the catalyst in a photocatalytic system [59].

The photocatalytic activity of synthesized ZnO nanoparticles was examined using methylene blue (MB) as the indicator. Sunlight was used as the light source. The reaction process is monitored spectrophotometrically by measuring the degradation of MB, which exhibits an apparent spectral profile with an absorption maximum at 667 nm. From Fig. 12, it is clear that the concentration of MB decreases dramatically while catalyzed using synthesized ZnO nanoparticles. The C/C_0 curves as a function of time are plotted in Fig. 13; synthesized ZnO photocatalysts can effectively remove the MB. Kinetic value is an

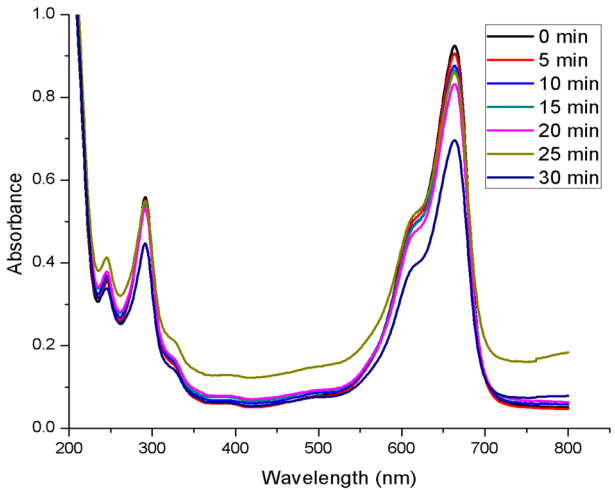

Fig. 12 Absorbance spectra of MB in the presence of ZnO nanoparticles

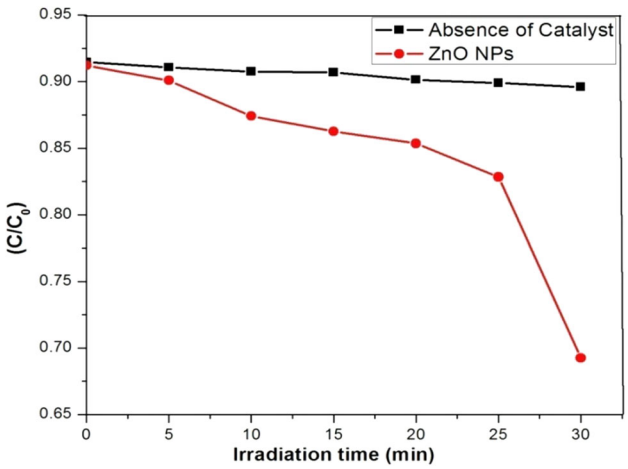

Fig. 13 The C/C_0 versus time curves of MB

important parameter for the photocatalyst. The kinetic curve shows linear relationships with time and can be fitted using the kinetic equation $\ln(C/C_0) = -k$, demonstrating that the photodegradation reaction in MB can be considered as a pseudo-first-order reaction, suggesting that ZnO

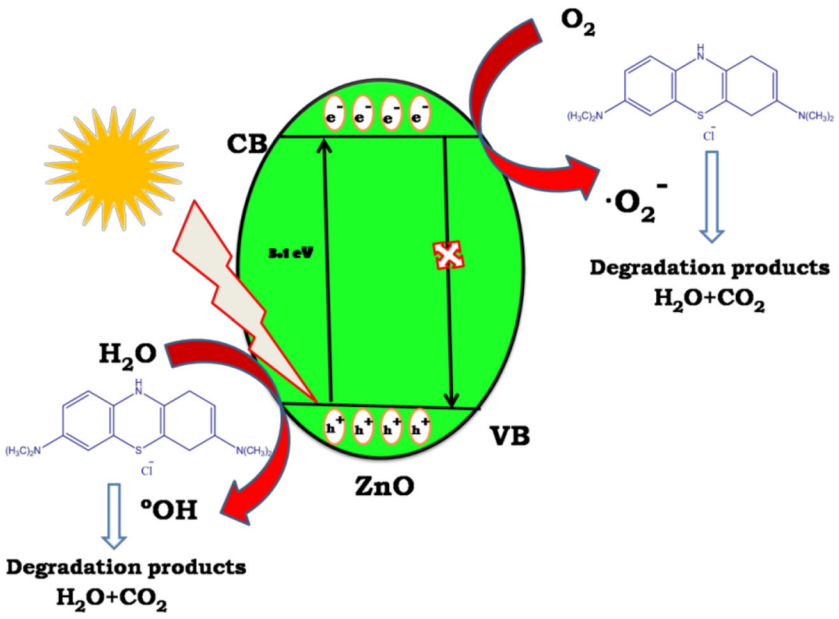

Fig. 14 Schematic diagram of photocatalytic mechanism of ZnO nanoparticles

nanoparticles have significant photocatalytic effects. The significant photocatalytic efficiency of ZnO nanoparticles is schematically illustrated in Fig. 14. Semiconductors have the similar band gaps 3.2 and 3.3 eV [60]. When the photocatalysts were irradiated by sunlight with the photon energy hν that exceeded the band gap energy of ZnO shown as 3.19 eV in Fig. 1b, electrons could be excited to the conductions band (CB) from the valence band (VB), simultaneously leaving the same number of holes behind in the VB. The holes and electrons would react with H_2O and oxygen dissolved in water which were adsorbed at the surface of ZnO nanoparticles and generated hydroxyl radicals ($^{\circ}OH$) and superoxide anion radicals (O^{2-}). These OH radicals and superoxide anion radicals are decomposing MB dye in the aqueous solution.

Pictorial representation of the photocatalytic activity of ZnO NPs for the degradation of organic dye (MB) is shown in Fig. 8. Under sunlight irradiation, the absorption of a photon of energy equal or higher than the ZnO band gap energy creates an electron and a hole on the surface. Then, the defects benefit the efficient separation of the generation of the (e^-/h^+) pairs, the photogenerated electrons reacted with O^2 or oxygen species to produce superoxide anion radicals, whereas the photogenerated holes reacted with water molecules to generate the hydroxyl radicals. Both radicals are oxidizing species in the photocatalytic oxidation processes [61]. The amount of energy possessed by the ZnO NPs is not sufficient to excite the electrons from valence band to conduction band. Catalyst needs certain amount of additional energy to excite the electrons from valence band to conduction band. When ZnO NPs are exposed to light, it absorbs energy. The excitation of electron takes place only when the amount of energy absorbed by ZnO NPs is more than the band gap. The formation of holes and electrons in the valence band and conduction band plays a major role in the degradation of dyes.

This activity influenced by various crucial factors like phase structure, surface area, optical absorption and separation efficiency of photogenerated charge carriers [62]. Surface increases defects extensively reduced by direct recombination of photogenerated electron–hole pair, development to the photocatalytic activity [63]. Photon-induced electron hole pairs assist in the redox reactions against the catalyst surface and produce superoxide ions and hydroxyl free radicals. These generated radicals act as powerful oxidize to disintegrate pollutant chemicals (dye) in wastewater [64]. This infects that the synthesis of ZnO NPs was effectively dye-degraded under sunlight. In plant-mediated (*Vitex trifolia L.*) synthesis of ZnO NPs, maximum decoloration efficiency occurred by 90 min with 30 mg of ZnO NPs catalyst dose [63], but *I. pes-caprae* aqueous leaf extract-mediated ZnO NPs maximum decoloration efficiency occurred by 90 min with 30 mg of ZnO NPs catalyst dose. Therefore, they indicate that the application can be extended in water treatment plants and textile industries.

Conclusion

The phytoconstituents such as flavonoids, phenolics, amino acids, steroids, proteins, carbohydrate and terpenoid present in the extract may act as reducing agents for the preparation of ZnO NPs and the capping of ZnO NPs by the phytoconstituents provide stability to ZnO NPs as

evident from FTIR studies. ZnO NPs have been prepared by using simple solution method via a green synthesis route. The synthesized ZnO NPs were found to have a crystalline structure with hexagonal wurtzite as evidenced by XRD method. The FE-SEM image studies have shown that the synthesized ZnO NPs are around 25 nm of nanodumbbell. The results proved that the ZnO NPs may serve as a potential antimicrobial agent. The cytotoxic effect of ZnO NPs showed high level of cytotoxic activity against the tested cancer cell lines. Hence, the results together suggest that the synthesized ZnO NPs would play a major role in target-based active molecules into specific cancer cells. The explored eco-friendly high-efficient ZnO NPs prepared from *Ipomoea pes-caprae* aqueous leaf extract are expected to have more extensive application in the medical field.

Acknowledgements Funding was provided by Adi Dravidar Welfare Scholarship (Govt. of Tamil Nadu).

Compliance with ethical standards

Conflict of interest The authors declare that they have no conflicts of interest with the contents of this article.

References

1. Del Campo J, Amiot MJ, Nguyen CJ (2000) Antimicrobial effect of *Rosemary* extract. Food Protect 63(10):1359–1368
2. Stary F, Hans S (1998) The national guides to medical herbs and plants. Tiger Books. Int. Plc, Twickenham
3. Xiong D, Fang T, Yu L, Sima X, Zhu W (2011) Effect of nano-scale TiO_2, ZnO and their bulk counterparts on zebrafish: acute toxicity, oxidative stress and oxidative damge. Sci Total Environ 409:1444. doi:10.1016/j.scitotenv.2011.01.015
4. Rasmussen JW, Martinez E, Louka P, Wingett DG (2010) Zinc oxide nanoparticles for selective destruction of tumor cells and potential for drug delivery applications. Drug Deliv 7(9):1063–1077. doi:10.1517/17425247.2010.502560
5. Seigneuric R, Markey L, Nuyten DSA, Dubernet C, Evelo CTA, Finot E, Garrido C (2010) From nanotechnology to nanomedicine: applications to cancer research. Curr Mol Med 10:640–652. doi:10.2174/156652410792630634
6. Rosarin FS, Arulmozhi V, Nagarajan S, Mirunalini S (2012) Antiproliferative effect of silver nanoparticles synthesized using *Amla* on Hep2 cell line. Asian Pac J Trop Med. doi:10.1016/S1995-7645(12)60193-X
7. Akhtar MJ, Ahamed M, Kumar S, Khan MM, Ahmad J, Alrokayan SA (2012) Zinc oxide nanoparticles selectively induce apoptosis in human cancer cellsthrough reactive oxygen species. Int J Nanomed 7:845–857. doi:10.2147/IJN.S29129
8. Buerki-Thurnherr T, Xiao L, Diener L, Arslan O, Hirsch C, Maeder-Althaus X, Grieder K, Wampfler B, Mathur S, Wick P, Krug HF (2013) In vitro mechanisticstudy towards a better understanding of ZnO nanoparticle toxicity. Nanotoxicology 7:402–416. doi:10.3109/1743590.2012.666575
9. Wahab R, Dwivedi S, Umar A, Singh S, Hwang IH, Shin HS, Musarrat J, Al-Khedhairy AA, Kim YS (2013) ZnO nanoparticles induce oxidative stress in Cloud man S91 melanoma cancer cells. J Biomed Nanotechnol 9:441–449. doi:10.1166/jbn.2013.1593
10. Shen C, James SA, de Jonge MD, Turney TW, Wright PF, Feltis BN (2013) Relating cytotoxicity zinc ions, and reactive oxygen in ZnO nanoparticle-exposed human immune cells. Toxicol Sci 136:120–130. doi:10.1093/toxsci/kft187
11. Deng Y, Zhang H (2013) The synergistic effect and mechanism of doxorubicin-ZnO nanocomplexes as a multimodal agent integrating diverse anticancer therapeutics. Int J Nanomed 8:1835–1841. doi:10.2147/IJN.S43657
12. Ajitha B, Reddy YAK, Reddy PS (2012) Green synthesis and characterization of silver nanoparticles using *Lantana camara* leaf extract. Mater Sci Eng, C 49:373–381. doi:10.1016/j.msec.2015.01.035
13. Valli JS, Vaseeharan B (2012) Biosynthesis of silver nanoparticles by *Cissus quadrangularis* extracts. Mater Lett 82:171–173. doi:10.1016/j.matlet.2012.05.040
14. Ladj R, Bit A, Eissa M, Mugnier Y, Le Dantec R, Fessi H, Elaissari A (2013) Individual inorganic nanoparticles: preparation, functionalization and in vitro biomedical diagnostic applications. J Mater Chem B 1:1381–1396. doi:10.1039/c2tb00301e
15. Vanathi P, Rajiv P, Narendhran S, Rajeshwari S, Pattanathu KSM, Venckatesh R (2014) Biosynthesis and characterization of phytomediated zinc oxide nanoparticles: a green chemistry approach. Mater Lett 134:13–15. doi:10.1016/j.matlet.2014.07.029
16. Zelechowska K, Golec JK, Karczewski J, Los M, Andrzej M, Kłonkowski M, Węgrzyn G, Golec P (2016) Phage-Directed synthesis of photoluminescent zinc oxide nanoparticles under benign conditions. Bioconjugate Chem 27:1999–2006. doi:10.1021/acs.bioconjchem.6b00196
17. Patra JK, Das G, Baek KH (2016) Phyto-mediated biosynthesis of silver nanoparticles using the rind extract of watermelon (*Citrullus lanatus*) under photo-catalyzed condition and investigation of its antibacterial, anticandidal and antioxidant efficacy. J Photochem Photobiol, B 161:200–210. doi:10.1016/j.jphotobiol.2016.05.021
18. Arumugam A, Karthikeyan C, Haja Hameed AS, Gopinath K, Gowri S, Karthika V (2015) Synthesis of cerium oxide nanoparticles using *Gloriosa superba L.* leaf extract and their structural, optical and antibacterial properties. Mater Sci Eng, C 49:408–415. doi:10.1016/j.msec.2015.01.042
19. Oppenlander T (2003) Photochemical purification of water and air. Wiley-VCH, Weinheim
20. Anpo M (2000) Utilization of TiO_2 photocatalysts in green chemistry. Pure Appl Chem 72:1265–1270
21. Fujishima A, Zhang X, Tryk D (2008) TiO2 photocatalysis and related surface phenomena. Surface Sci Rep. 63:515–582. doi:10.1016/j.surfrep.2008.10.001
22. Lin D, Wu H, Zhang R, Pan W (2009) Enhanced photocatalysis of electrospun Ag–ZnO heterostructured nanofibers. Chem Mater 21:2479–3484. doi:10.1021/cm900225p
23. Hassan SSM, El Azab WIM, Ali HR, Mansour MS (2015) Green synthesis and characterization of ZnO nanoparticles for photocatalytic degradation of anthracene. Adv Nat Sci Nanosci Nanotechnol 6:11. doi:10.1088/2043-6262/6/4/045012
24. Antoine TE, Mishra YK, Trigilio J, Tiwari V, Adelung R, Shukla D (2010) Prophylactic, therapeutic and neutralizing effects of zinc oxide tetrapod structures against herpes simplex virus type-2 infection. Antivir Res 96:363–375. doi:10.1016/j.antiviral.2012.09.020
25. Hong D, Zang W, Guo X, Fu Y, He H, Sun J, Xing L, Liu B, Xue X (2016) High piezo-photocatalytic efficiency of CuS/ZnO nanowires using both solar and mechanical energy for degrading organic dye. ACS Appl Mater Interfaces 8(33):21302–21314. doi:10.1021/acsami.6b05252
26. Krishnaraj C, Jagan EG, Rajasekar S, Selvakumar P, Kalaichelvan PT, Mohan N (2010) Synthesis of silver nanoparticles using

Acalypha indica leaf extracts and its antimicrobial activity against water borne pathogens. Colloids Surf B Biointerfaces 76(1):50–56. doi:10.1016/j.colsurfb.2009.10.008
27. Sheny DS, Mathew J, Philip D (2011) Phytosynthesis of Au, Ag and Au–Ag bimetallic nanoparticles using aqueous extract and dried leaf of *Anacardium occidentale*. Spectrochim Acta A Mol Biomol Spectr 79(1):254–262. doi:10.1016/j.saa.2011.02.051
28. Xu X, Chen D, Yi Z, Jiang M, Wang L, Zhou Z, Fan X, Wang Y, Hui D (2013) Antimicrobial mechanism based on H_2O_2 generation at oxygen vacancies in ZnO crystals. Langmuir 29(18):5573–5580. doi:10.1021/la400378t
29. Elumalai K, Velmurugan S, Ravi S, Kathiravan V, Ashokkumar S (2015) Bio-fabrication of zinc oxide nanoparticles using leaf extract of curry leaf (Murraya koenigii) and its antimicrobial activities. Mater Sci Semicond Proces 34:365–372. doi:10.1016/j.mssp.2015.01.048
30. Devall MS (1992) The biological flora of coastal dunes and wetlands. *Ipomoea pes-caprae* (L.) Roth. J Coastal Res 8:442–456
31. Agoramoorthy G, Chen FA, Venkatesalu V, Kuo DH, Shea PC (2008) Evaluation of antioxidant polyphenols from selected mangrove plants of India. Asian J Chem 20(2):1311–1322
32. Premanathan M, Nakashima H, Kathiresan K, Rajendran N, Yamamoto N (1996) In vitro anti human immuno deficiency virus activity of mangrove plants. Indian J Med Res 130:276–279
33. Onwukeame DM, Ikuegbvweha TB, Asonye CC (2007) Evaluation of phytochemical constituents, antibacterial activities and effects of exudates of *Pycanthus angolensis* weld warb (mysristicaeceae) on corneal ulcers in rabbit. Trop J Pharm Res 6(2):725–730
34. Barreira JCM, Ferreira ICFR, Oliveira MBPP, Pereira J (2008) A Antioxidant activities of the extracts from chestnut flower, leaf, skins and fruit. Food Chem 107:1106–1113. doi:10.1016/j.foodchem.2007.09.030
35. Grubesic RJ, Vukovic J, Kremer D, Vladimir-knezevic S (2005) Spectroscopic method for polyphenols analysis. Prevalidation and application on plantogo L. species. J Pharmaceut Biomed 39:837–842. doi:10.1016/j.ipba.2005.05.004
36. Oyaizu M (1986) Studies on the product of browning reaction prepared from glucose amine. Jap J Nat 44:307–315
37. Stan M, Popa A, Toloman D, Silipas TD, Vodnar DC (2016) Antibacterial and antioxidant activities of ZnO nanoparticles synthesized using extracts of *Allium sativum, Rosmarinus officinalis and Ocimum basilicum*. Acta Metall Sin (Engl Lett) 29:228–236. doi:10.1007/s40195-016-0380-7
38. Srinivasan R, Natarajan D, Shivakumar MS (2014) Antimicrobial and GC-MS analysis of *Memecylon edule* leaf extracts. *Int J Curr Pharm Rev and Res* 5:1–13. ISSN: 0976-822X
39. Selvakumaran M, Pisarcik DA, Bao R, Yeung AT, Hamilton TC (2003) Enhanced cisplatin cytotoxicity by disturbing the nucleotide excision repair pathway in ovarian cancer cell lines. Cancer Res 63:1311–1316
40. Brousseau P, Payette Y, Tryphonas H, Blakley B, Flipo D, Fournier M (1999) Assessment of cell viability: determination of cell viability and cell concentration with ethidium bromide and acridine orange. In: Beudet M, Kouassi E, Lapierre P, Voccia I (eds) Manual of immunological methods. CRC Press LLC, Boca Raton, pp 28–29
41. Ribble D, Goldstein NB, Norris DA, Shellman YG (2005) Simple technique for quantifying apoptosis in 96-well plates. BMC Biotechnol 5(12):1–7. doi:10.1186/1472-6750-5-12
42. Vijayan P, Viswanathamurthi P, Sugumar P, Ponnuswamy MN, Balakumaran MD, Kalaichelvan PT, Velmurugan K, Raju N, Butchere RJ (2015) Unprecedented formation of organo-ruthenium(II) complexes containing 2-hydroxy-1-naphthaldehyde S-benzyldithiocarbazate: synthesis, X-ray crystal structure, DFT study and biological activities in vitro. Inorg Chem Front. doi:10.1039/C5QI00029G
43. Parthibana C, Sundaramurthy N (2015) Biosynthesis, characterization of ZnO nanoparticles by using *Pyrus pyrifolia* leaf extract and their photocatalytic activity. IJIRSET 10:9710–9718. doi:10.15680/IJIRSET.2015.0410031
44. Iravani S, Korbekandi H, Mirmohammadi SV, Zolfaghari B (2014) Synthesis of silver nanoparticles: chemical, physical and biological methods. Res Pharm Sci 9:385–406
45. Kharat SN, Mendhulkar VD (2016) Synthesis, characterization and studies on antioxidant activity of silver nanoparticles using *Elephantopus scaber* leaf extract. Mat Sci Eng C 62:719–724. doi:10.1016/j.msec.2016.02.024
46. Senthilkumar SR, Sivakumar T (2014) Green tea (*Camellia sinensis*) mediated synthesis of zinc oxide nanoparticles and studies on their antimicrobial activities. Int J Pharm Pharm Sci 6:461–465
47. Yu ZJ, Rajesh Kumar M, Sun DL, Wang LT, Hong RY (2016) Large scale production of hexagonal ZnO nanoparticles using PVP as a surfactant. Mater Lett 166:284–287. doi:10.1016/j.matlet.2015.12.102
48. Mittal AK, Kaler A, Banerjee UC (2012) Free radical scavenging and antioxidant activity of silver nanoparticles synthesized from flower extract of *Rhododendron dauricum*. Nano Biomed Eng 4:118–124. doi:10.5101/nbe.v4i3.p118-124
49. John Sushma N, Mahitha B, Mallikarjuna K, Prasad Raju BD (2016) Bio-inspired ZnO nanoparticles from *Ocimum tenuiflorum* and their in vitro antioxidant activity. Appl Phys 122:544. doi:10.1007/s00339-016-0069-9
50. Sathishkumar G, Pradeep K, Jha B, Vignesh V, Rajkuberan C, Jeyaraj M, Selvakumar M, Jha R, Sivaramakrishnan S (2016) Cannonball fruit (*Couroupita guianensis, Aubl*.) Cannonball fruit (*Couroupita guianensis, Aubl*) extract mediated synthesis of gold nanoparticles and evaluation of its antioxidant activity. J Mol Liq 215:229–236. doi:10.1016/molliq.2015.12.043
51. Subramanian R, Subbramaniyan P, Raj V (2013) Antioxidant activity of the stem bark of *Shorea roxburghii* and its silver reducing power. Springer Plus 2:28. doi:10.1186/2193-1801-2-28
52. Kong H, Yang J, Zhang Y, Fang Y, Nishinari K, Phillips GO (2014) Synthesis and antioxidant properties of gum arabic-stabilized selenium nanoparticles. Int J Biol Macromol 65:155–162. doi:10.1016/j.ijbiomac.2014.01.011
53. Das D, Nath BC, Phukon P, Dolui SK (2013) Synthesis and evaluation of antioxidant and antibacterial behavior of CuO nanoparticles. Colloids Surf B 101:430–433. doi:10.1016/j.colsurfb.2012.07.002
54. Indra Priyadharshini R, Prasannaraj G, Geetha N, Venkatachalam P (2014) Microwave-mediated extracellular synthesis of metallic silver and zinc oxide nanoparticles using macro-algae (*gracilaria edulis*) extracts and its anticancer activity against human PC3 cell lines. Appl Biochem Biotechnol 174(8):2777–2790. doi:10.1007/s12010-014-1225-3
55. Suresh D, Nethravathi PC, Udayabhanu Rajanaika H, Nagabhushana H, Sharma SC (2015) Green synthesis of multifunctional zinc oxide nanoparticles using *Cassia fistula* plant extract and their photodegradative, antioxidant and antibacterial activities. Mater Sci Semiconduct Process 31:446–454. doi:10.1016/j.mssp.2014.12.023
56. Selvakumari R, Deepa V, Mahalakshmi P, Subhashini N, Lakshminarayan (2015) Anti cancer activity of ZnO nanoparticles on MCF7 (breast cancer cell) and A549 (lung cancer cell). ARPN J Eng Appl Sci 10:5418–5421. ISSN 1819-6608
57. Vermes I, Haanen C (1994) Apoptosis and programmed cell death in health and disease. Adv Clin Chem 31:177–246 **PMID: 7879672**

58. Savill JS, Henson PM, Henson JE, Haslett C, Walport MJ, Wyllie AH (1989) Macrophage phagocytosis of aging neutrophils in inflammation. Programmed cell death in the neutrophil leads to its recognition by macrophages. J Clin Invest 83:865–875. doi:10.1172/jci113970
59. Etacheri V, Roshan R, Kumar V (2012) Mg-doped ZnO nanoparticles for efficient Sunlight-driven photocatalysis. ACS Appl Mater Interfaces 4:2717–2725. doi:10.1021/am300359h
60. Wang Y, He Y, Li T, Cai J, Luo M, Zhao L (2012) Novel $CaBi_6O_{10}$ photocatalyst for methylene blue degradation under visible light irradiation. Catal Commun 18:161–164. doi:10.1016/j.catcom.2011.12.011
61. Manjunath K, Ravishankar TN, Kumar D, Priyanka KP, Varghese T, Raja Naika H, Nagabhushana H, Sharma SC, Dupont J, Ramakrishnappa T, Nagaraju G (2014) Facile combustion synthesis of Zno nanoparticles using *Cajanus cajan* (L.) and its multidisciplinary application. Mater Res Bull 57:325–334. doi:10.1016/j.materresbull.2014.06.010
62. Jyoti Prakash D, Braja Gopal M, Garudadhwaj H (2015) Hydrothermal synthesis and enhanced photocatalytic activity of ternary $Fe_2O_3/ZnFe_2O_4/ZnO$ nanocomposite through cascade electron transfer. RSC Adv 5:58072–58083. doi:10.1039/C5RA05894E
63. Elumalai K, Velmurugan S, Ravi S, Kathiravan V, Ashokkumar S (2015) Bio-fabrication of zinc oxide nanoparticles using leaf extract of curry leaf (*Murraya koenigii*) and its antimicrobial activities. Mater Sci Semiconduct Process 34:365–372. doi:10.1016/j.mssp.2015.01.08
64. Dawood S, Sen TK (2014) Review on dye removal from its aqueous solution into alternative cost effective and non-conventional adsorbents. J Chem Proc Engg 1:1–11